Superallowed Gamow-Teller Decay of Doubly Magic ^{100}Sn

C. Hinke, M. Böhmer, P. Boutachkov, T. Faestermann, H. Geissel, R. Gernhäuser, M. Górska, A. Gottardo, H. Grawe, J. Gręboszz, R. Krücken, N. Kurz, Z. Liu, L. Maier, F. Nowacki, S. Pietri, Zs. Podolyák, K. Sieja, K. Steiger, K. Straub, H. Weick, P. J. Woods, N. Al-Dahan, N. Alkhomashi, A. Atac, A. Blazhev, N. Braun, I. Čeliković, T. Davinson, I. Dillmann, C. Domingo-Pardo, P. Doornenbal, G. de France, G. Farelli, F. Farinon, J. Gerl, N. Goel, T. Habermann, R. Hoischen, R. Janik, M. Karny, A. Kaskas, I. Kojouharov, Th. Kröll, Y. Litvinov, S. Myalski, F. Nebel, S. Nishimura, C. Nociforo, J. Nyberg, A. Parikh, A. Procházka, P. H. Regan, C. Rigollet, H. Schaffner, C. Scheidenberger, S. Schwertel, P. -A. Söderström, S. Steer, A. Stolz, P. Strmeň, H.-J. Wollersheim

Abstract

abstract

v. 26.09.2011

Author contributions:

Fragment separator: H.W., P.B., H.Ge., M.G., Z.P.; particle detectors: C.H., K.Str., R.G., T.F., L.M., F.Ne.; RISING γ-array: P.B., M.G., S.P., J.Ge., H.-J.W.; data acquisition and analysis software: M.B., R.G., J.Gr., N.K., L.M.; data analysis and interpretation: C.H., K.Str., T.F., M.G., H.Gr., R.K., K.Ste., F.No., K.Si.; writing of manuscript: C.H., R.K., T.F., R.G.; all authors except H.Gr., F.No., K.Si. took part in the preparation and the beam times and commented on the final paper.

PACS numbers:

I. SUMMARY

The shell structure of atomic nuclei is associated with magic numbers and originates from the nearly independent motion of neutrons and protons in a mean potential generated by all nucleons. During beta decay, induced by weak interaction, a proton (neutron) in an occupied orbital decays into a neutron (proton) in a previously unoccupied orbital. During the decay the nucleon spin may remain the same (Fermi) or may be flipped (Gamow-Teller (GT)). It is only partially understood why matrix elements of spin-operators, such as the ones for GT and magnetic transitions and moments, are systematically reduced in the nuclear medium compared to the single particle values. This renormalisation is often taken into account by using an effective operator. This is of wider importance since GT beta-decay matrix elements are relevant in various astrophysical scenarios as well as for double-beta decay[1, 2].

In most nuclei measuring the full GT strength is difficult since it is quite fragmented and only partially accessible in β-decays. ^{100}Sn, the heaviest doubly magic nucleus with equal proton and neutron number, is unique since the decay is predicted to dominantly populate a single state. We measured half-life and Q-value for the GT decay of ^{100}Sn. We find the smallest log-ft value of all known beta-decays and a large GT strength establishing it as superallowed GT decay. Large scale shell model calculations that include up to five particle-hole excitations incorporating the well established renormalisation due to short range correlations (higher-order effect) allow for a consistent description of the observed GT-strength for this unique showcase nucleus providing firm and conclusive evidence for the robust N=Z=50 shell closures at ^{100}Sn .

II. INTRODUCTION

GT-transitions, in which a proton (neutron) is transformed into a neutron (proton) while at the same time flipping its spin, are an important spin-isospin degree of freedom in atomic nuclei. Most of the GT-strength is found in the collective Gamow-Teller Giant Resonance (GTGR), which is typically a broad structure fragmented over many states. Experiments investigating the GT-strength via β-decay or charge exchange reactions observed only about half of the total Ikeda sum-rule [3] in many nuclei. This phenomenon is referred to as *GT-quenching* [4, 5] and has been intensively discussed. The most popular mechanisms for

the GT-quenching are particle-hole correlations moving strength to energies at 20-50 MeV, substantially above the GTGR, or the coupling to Δ-hole excitations (where a nucleon is excited to the Δ-resonance) moving strength to energies above 300 MeV. Recently new (p,n) and (n,p) reaction studies have indeed discovered substantial amounts of GT-strength as high as 50 MeV such that about 85-90 % of the sum-rule is exhausted, leaving little room for Δ-hole excitations [6]. In most calculations that involve truncated model spaces or the full major oscillator shell a GT-operator renormalized by a factor $\approx (1/1.26)$ is used, setting artificially the weak coupling constants $g_A \approx g_V$, to account for correlations not included in the model space. While in charge exchange reactions the full GTGR is accessible, β-decay studies can only observe the fraction of the total GT-strength within the decay energy window. Near the proton dripline this window becomes larger since the Coulomb repulsion shifts the proton levels up. Nevertheless, it is experimentally challenging to detect all small GT fragments [6, 7]. The doubly magic $N = Z$ nucleus ^{100}Sn provides an experimentally and theoretically very clean situation. The closed $N = 50$ and $Z = 50$ shells reduce the effect of long-range correlations, decreasing the amount of fragmentation of the GTGR. At the same time the energy window for beta decay is $\sim$ 7.4 MeV [8] and thus most of the GTGR is accessible. In an extreme single particle picture the only possible GT-transition is the decay of a proton in a completely filled $g_{9/2}$ shell to a neutron in an empty $g_{7/2}$ shell since all other final states are Pauli blocked and no levels above $Z = 50$ are occupied. This would lead to a GTGR consisting of only a single 1^+ level with a quenched GT-strength of $B_{GT} \approx 10$ taking into account the standard renormalisation factor of 0.75 of the GT matrix element originating from short-range correlations [9]. This unique situation is met nowhere else in the Segré chart and has been termed super-allowed GT-decay [10]. Even in more realistic models, including particle-hole correlations, the GT-decay of the ground state of ^{100}Sn is predicted to populate with more than 95% a single 1^+ state in ^{100}In at an excitation energy of about $3MeV$. In these calculations an unquenched B_{GT} of around 8-14 [11, 12, 13, 14] is obtained, leading to quenched predictions of 5-7 [12, 14].

The production and study of the decay properties of ^{100}Sn has been the aim of several experiments [15, 16, 17, 18, 19], where only a few ^{100}Sn nuclei were uniquely identified. Here we report on a new measurement of the half-life and Q-value from 259 identified ^{100}Sn nuclei resulting in the smallest log-ft value of any β-decay on the nuclear chart and a large GT-strength establishing the robustness of the N=Z=50 shell closure in ^{100}Sn.

III. EXPERIMENTAL DETAILS

The experiment was performed at the GSI Helmholtzzentrum Darmstadt, Germany. A ^{124}Xe beam of $E_{kin} = 1AGeV$ with one second long spills of $3 \cdot 10^9$ ions every three seconds was directed onto a beryllium target placed in front of the fragment separator (FRS) [20]. Proton-rich nuclei were produced via relativistic projectile fragmentation and guided to the final FRS focal plane while being identified event by event (see Figure 1). The correct identification was verified by observing the gamma radiation depopulating known isomers, e.g. the 8^+ isomer in ^{98}Cd. In total 259 ^{100}Sn nuclei were unambiguously identified, with a production rate of 0.75 per hour, yielding a production cross-section of $5.8(21)pb$.

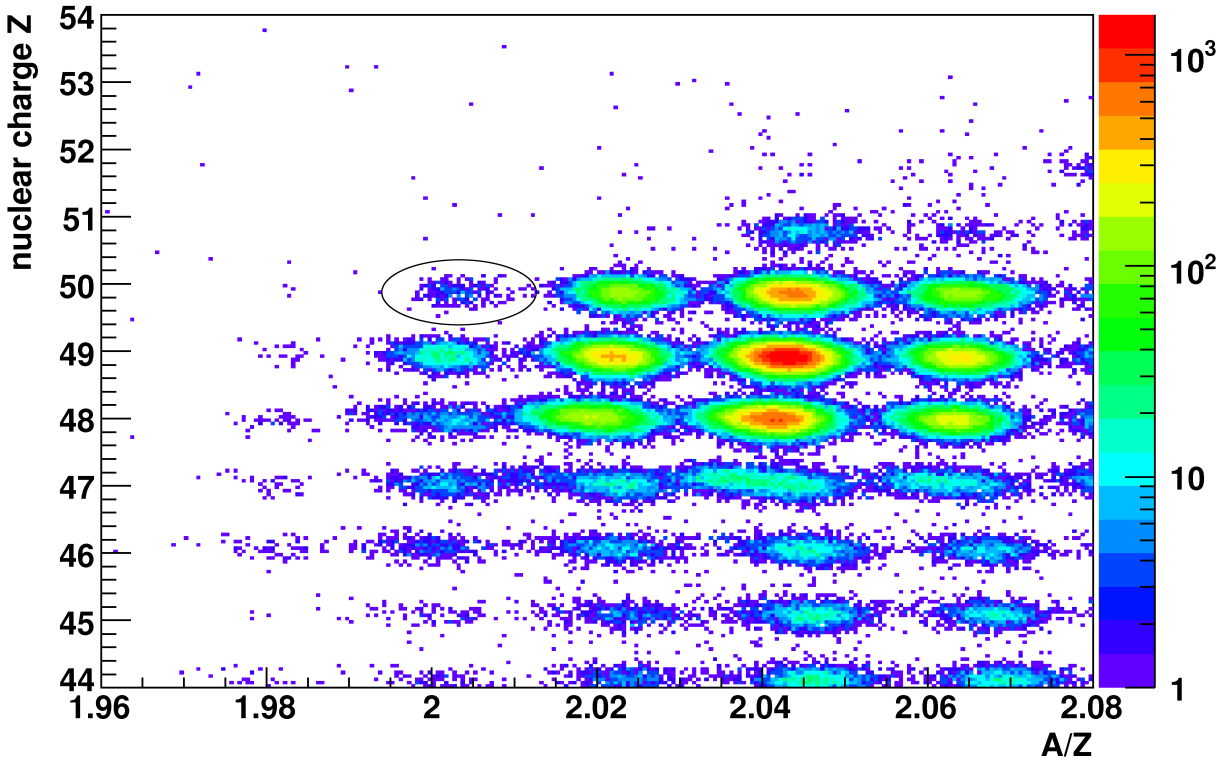

FIG. 1: Particle identification plot with respect to the nuclear charge Z and the mass-to-charge ratio A/Z for the full statistics of the ^{100}Sn fragment separator setting. In total 259 ^{100}Sn nuclei (indicated) have been unambiguously identified. Resolutions (FWHM) in mass of $\Delta A = 0.32$ and nuclear charge $\Delta Z = 0.25$ were obtained.

The ions were implanted into a stack of highly segmented silicon strip detectors which

was surrounded by the RISING array of 105 Germanium detectors in the stopped beam configuration [21] in order to detect emitted gamma rays with high efficiency.

IV. ANALYSIS AND RESULTS

Following a ^{100}Sn implantation in a pixel of the implantation zone all decay events were recorded that occurred within 15 seconds in this and the directly neighboring pixels in three dimensions. During this correlation time it was possible to assign 126 decay chains to 163 ^{100}Sn implantations. A maximum likelihood (MLH) analysis with a maximum of three decay events during the correlation time was used to analyze these decay chains. The half-life of ^{100}Sn was deduced as $1.16(20)s$ in the MLH analysis using literature values for the lifetimes of the daughter nuclei. The measurement is much more accurate than previous experiments yielding $0.94^{+0.54}_{-0.27}s$ [17] and $0.55^{+0.70}_{-0.31}s$ [19]. In Figure 2 the decay curve for ^{100}Sn is shown.

Figure 3 shows the gamma-ray spectrum observed in coincidence with decay events following ^{100}Sn implantations. The five newly observed transitions are associated with the depopulation of excited states in the daughter nucleus ^{100}In.

The statistics was only sufficient to establish a coincidence between the 436 keV and 96 keV transitions and thus it is impossible to deduce an unambiguous level scheme of ^{100}In. Within uncertainties the transitions could have the same intensity, which would allow for a single cascade of 5 transitions from the excited 1^+ state to the ground state. However, this would lead to an excitation energy of more than $4MeV$, which is higher than the $2.5(5)MeV$ predicted with realistic shell model calculations (see e.g. [22, 23]). The large uncertainties of the observed intensities also allow for two parallel cascades originating from this 1^+ state.

Figure 4 shows the relevant level scheme for ^{100}In obtained from large scale shell model calculations (LSSM). In this approach ^{100}Sn is not treated as an inert doubly-magic core but excitations across the Z=N=50 shell closure were allowed within the N=4 harmonic oscillator shell with an effective interaction derived from nucleon-nucleon potentials by a standard many-body approach for a ^{80}Zr core [24] (see supplementary section). The decay relevant states of two multiplets are shown, $(1^+, 2^+, 3^+)$ originating from the $\pi g^{-1}_{9/2} \otimes \nu g^1_{7/2}$ configuration and $(2^+, 3^+, 4^+, 5^+, 6^+)$ from the $\pi g^{-1}_{9/2} \otimes \nu d^1_{5/2}$ configuration. In this calculation it is assumed that the $\nu d_{5/2}$ level in ^{101}Sn lies 172 keV below the $\nu g_{7/2}$ level [25]. However, the final conclusions do not change if the reverse situation is assumed, as suggested in [26].

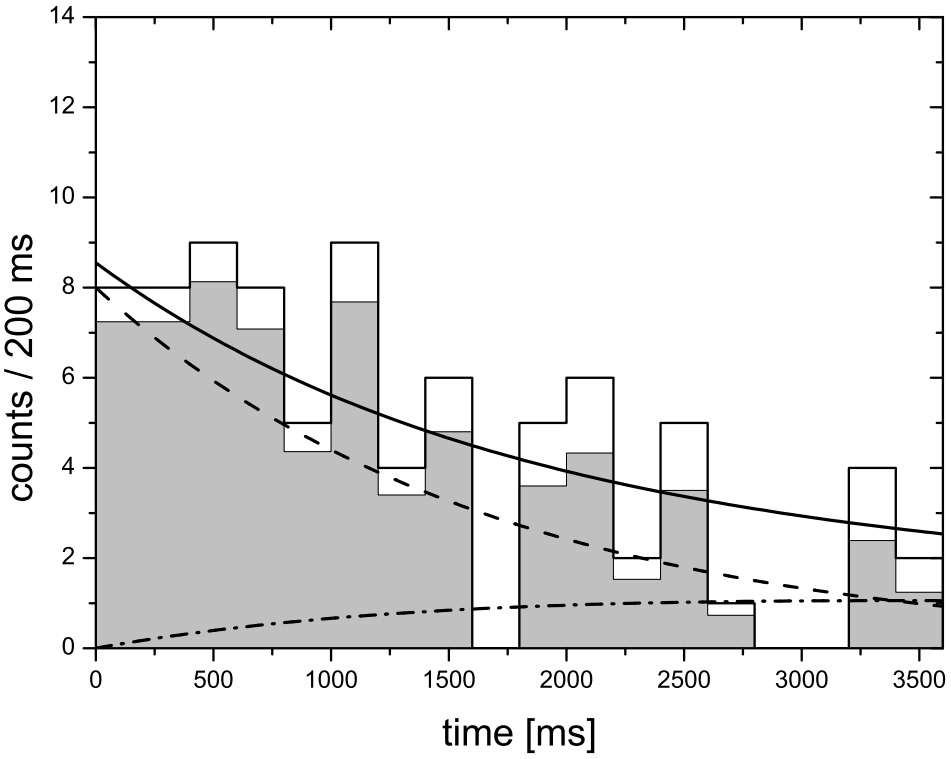

FIG. 2: Decay curve of ^{100}Sn according to the obtained half life together with the number of ^{100}Sn decays among all first decay events in 200ms time bins after implantation. Time distribution of first decays after the implantation of ^{100}Sn nuclei (solid line histogram). Decay curves resulting from the MLH analysis are shown individually for ^{100}Sn (dashed) and its daughter ^{100}In (dash-dotted) together with the sum of these decay curves (solid) taking into account a small amount of random background. The light gray filled histogram represents the actual ^{100}Sn content according to the MLH analysis.

The predictions reflect the observed gamma-ray transitions well if the high energy 2048 keV transition populates the lowest 2^+ state, which decays to lower lying states via the 436, 141, and 96 keV transitions ending either in the 6^+ ground state or a low lying isomeric state with unobserved decay. In this scenario the second 2^+ state is populated with the 1297 keV transition and decays to the lower lying 2^+ and 3^+ states. This may lead to a fragmentation of the intensities making it impossible to observe these transitions in the present experiment. This scenario is supported by the measurement of the total gamma-ray energy in a former

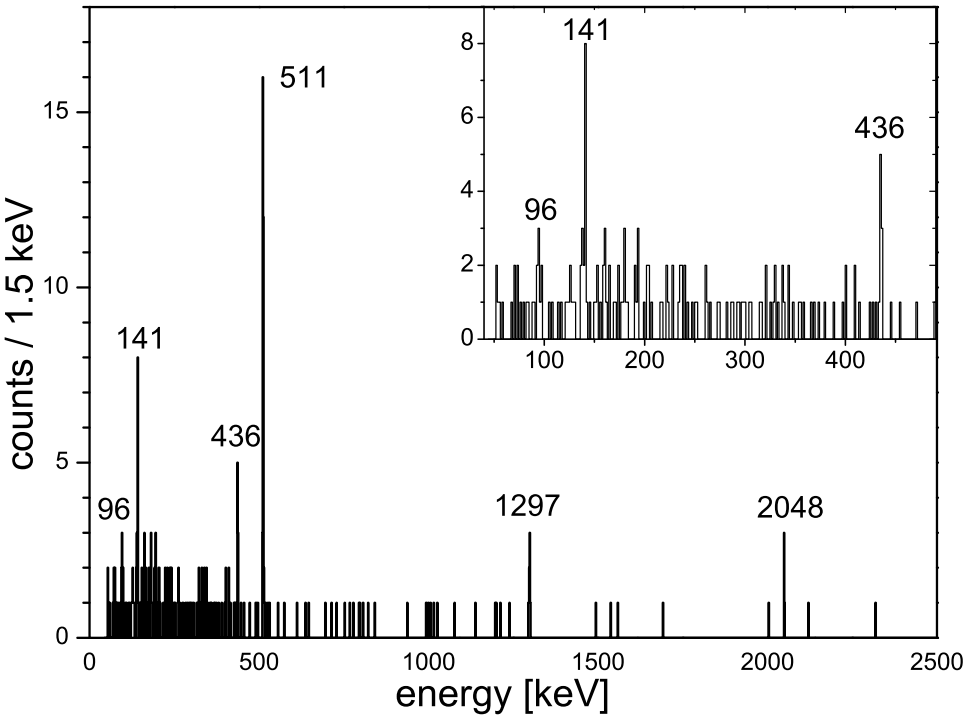

FIG. 3: Energy distribution of the gamma-radiation observed in coincidence with the beta decay of ^{100}Sn. The spectrum contains with a probability of 65% radiation directly following ^{100}Sn decay events. The other contributions are uncorrelated background decays and daughter decays of ^{100}In. None of the observed lines corresponds to known transitions from these minor contributions. The measured absolute intensities of the five lines with the energies 96, 141, 436, 1297 and 2048 keV are 79 ± 40, 100 ± 31, 59 ± 22, 72 ± 26 and 53 ± 26 corrected for the emission of conversion electrons assuming M1-transitions and 141±70, 122±37, 59±22, 72±26 and 53±26 assuming E2-transitions, respectively.

experiment with a BGO-detector [17], the known mass difference of ^{100}Sn and ^{100}In [16] and our observation of a single event of β-delayed proton emission and is fully consistent with the expectation that dominantly a single 1^+ state is populated in the decay. Further details are given in the supplementary section.

As a key feature of this experiment, the kinetic energy of the decay positrons fully absorbed in the compact silicon detector array was measured. The spectrum resulting from the

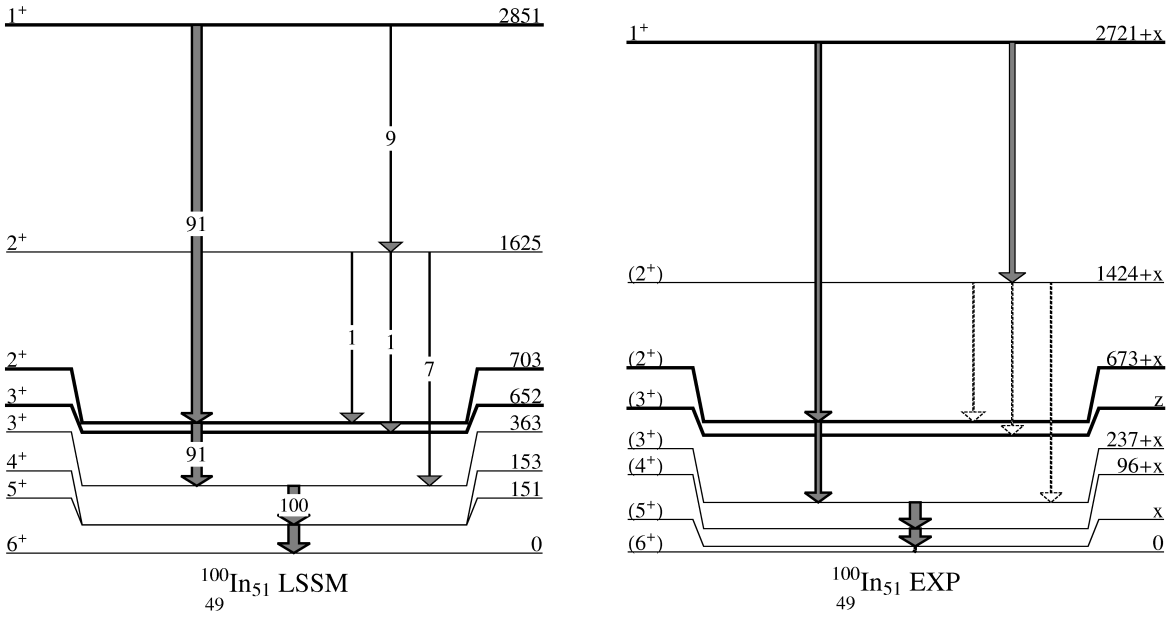

FIG. 4: *Left:* Large scale shell model (LSSM) calculation of the low lying excited states in ^{100}In. The energy of the states is given in keV and the quantum numbers denoting the states are spin and parity. Populated levels with almost pure $\pi g_{9/2}^{-1} \otimes \nu g_{7/2}^{1}$ configuration are indicated with bold lines while the remaining levels are part of the $\pi g_{9/2}^{-1} \otimes \nu d_{5/2}^{1}$ multiplet. Explicit numbers for the intensities of selected transitions relative to the strongest transition are shown. *Right:* Possible level scheme resulting from the most likely interpretation of the observed five gamma ray transitions in ^{100}In. Since at least one low energy transition might not have been observed in the cascade on the left if using only M1-transitions the energy of the levels might have a systematic shift up to $x = 80keV$ due to the experimental detection threshold. The dashed transitions are most likely below the detection limit of the experiment.

summed up energies of the uninterrupted β-traces up to three seconds after a ^{100}Sn implantation is shown in Figure 5. It was fitted using a MLH analysis based on a single component beta decay phase space function to determine the endpoint energy in the decay of ^{100}Sn. For the fit of the end point energy only data in the energy region between $400keV$ and $2600keV$ were used. In the analysis corrections were applied for the occurrence of converted low energy transitions emitted during the deexcitation of the daughter nucleus ^{100}In, for emitted Bremsstrahlung of the positrons, and for the annihilation of positrons in flight before the deposition of their total kinetic energy. The measured value of the endpoint energy of the β-decay populating a single final state in the daughter nucleus ^{100}In was determined to be

3.29(20)MeV. The corresponding fraction of electron capture decays was calculated to be 13% of all ^{100}Sn decays. Assuming the four lowest 1^+ states in ^{100}In with the energy splitting and the relative GT-strength from the LSSM calculation (see supplementary section), the measured beta-spectrum would yield an endpoint energy for the transition to the lowest 1^+ state that is larger by 73keV.

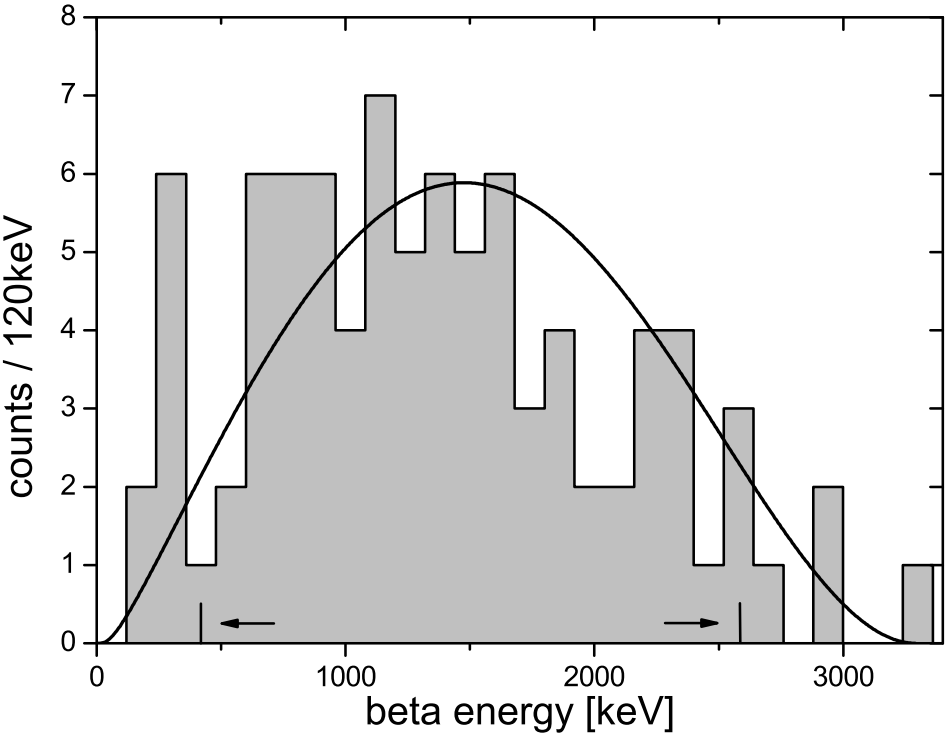

FIG. 5: Distribution of the positron energies emitted in the beta decay of ^{100}Sn. The spectrum contains only decay events which can be assigned to ^{100}Sn decays with a probability of at least 75%. The MLH fit was applied to the region between 400keV and 2600keV which is indicated with markers. The solid curve illustrates the shape of the best fitting single component beta decay phase space function determined in a MLH analysis.

V. DISCUSSION

Using the measured half-life and the end point energy a log-ft value of $2.62^{+0.13}_{-0.19}$ was extracted, which is the smallest known log-ft value for any beta decay in the nuclear chart.

Thus, the Gamov-Teller decay of ^{100}Sn has much larger strength than the known $0^+ \rightarrow 0^+$ superallowed Fermi decays of $N = Z$ nuclei and is indeed a *superallowed Gamow-Teller decay* [27]. The extracted Gamow-Teller strength B_{GT} of the ^{100}Sn ground state decay to the single excited 1^+ state in ^{100}In is $B_{GT} = 9.1^{+4.8}_{-2.3}$. This is surprisingly large but within uncertainties still consistent with the value of $B_{GT} = 5.8^{+5.5}_{-3.2}$ deduced from previous results of Q_{EC} and $T_{1/2}$ [28]. The uncertainty of the new B_{GT} value is dominated by the uncertainty of the beta endpoint energy. The extraction of the strength was performed under the assumption of the GT-decay into only one final 1^+ state in ^{100}In. However, if other 1^+ states at excitation energies above the observed state would also be populated, the summed GT-strength would only increase while the B_{GT} for the first excited 1^+ state would decrease. It would have been difficult to observe such states since the reduced phase space for higher lying 1^+ states would have lead to a strongly reduced population.

The LSSM calculations which take into account long-range correlations across the N=Z=50 doubly magic shell closure and include up to five particle-hole excitations (see supplementary section for details) yield a total summed GT-strength of all possible final states in the daughter nucleus up to $60MeV$ of $B_{GT} = 8.19$ applying the standard renormalisation due to short-range correlations.

This quenching of the GT-strength takes into account those correlations not included in the model space, in particular higher energy particle-hole excitations or excitation of the Δ resonance. Higher-order correlations from beyond the 0 $\hbar\omega$ valence space are well documented in the N=1,2,3 p, sd, pf harmonic oscillator shells [9] amounting to a reduction of the GT matrix element by a factor of about 0.75 in medium-heavy nuclei. This is a property of the wave functions and in line with evidence for the M1 operator and spectroscopic factors (see Ref.[9] for a summary). Their absence or reduction in the N=4 gds shell therefore is unlikely.

A quenched GT-strength of $B_{GT} = 7.82$ is predicted in the experimental Q_{EC} window of 7.03(20) MeV. This corresponds to a reduction of the total renormalised GT strength of the extreme single particle estimate of $B_{GT} \approx 10$ by 18% for excitation energies up to $60MeV$ and by 22% in the Q_{EC} window. It is due to mixing in the gds harmonic oscillator shell, i.e. emptying of the proton $g_{9/2}$ orbital and pre-filling of the neutron $g_{7/2}$ orbital. The occupation numbers of the two orbitals which are linked by the GT operator of course directly influence the strength of the transition matrix element.

However, the prediction is that the largest fraction of the strength remains located in the first excited 1^+ state which agrees with earlier calculations [11, 27]. Nevertheless, according to the LSSM calculations performed in this work it is reasonable to consider that several 1^+ states in ^{100}In are populated in the decay of ^{100}Sn. If we take from the LSSM calculation the four lowest 1^+ states in ^{100}In with their energy splitting and relative GT-strength (see supplementary section), the value of $B_{GT}(1^+_1) = 9.1^{+4.8}_{-2.3}$ (assuming a single 1^+ state) would be reduced to $B_{GT}(1^+_1) = 7.6^{+2.6}_{-2.1}$ for the first excited 1^+ state using the experimental log-ft value. The corresponding summed GT-strength would be $\sum_{i=1}^{4} B_{GT}(1^+_i) = 9.9^{+3.4}_{-2.8}$ using the experimental log-ft value and the theoretical distribution of strength.

The quenched LSSM result of $B_{GT} = 5.68$ of the GT-strength for this first excited 1^+ state agrees well with the value $B_{GT} = 7.6^{+2.6}_{-2.1}$ within the statistical uncertainty extracted from the experimental log-ft value under above assumptions. The experimental concentration of most of the GT strength in the first excited 1^+ state with marginal fragmentation clearly classifies the ^{100}Sn GT decay as super-allowed. The calculation shows that the large GT-strength of the first excited 1^+ state coincides with relatively pure wave functions of the ^{100}Sn ground state and of the first excited 1^+ state in ^{100}In consisting significantly of the $g^{10}_{9/2} \otimes g^{0}_{7/2}$ $(xxx\%)$ and the $g^{9}_{9/2} \otimes g^{1}_{7/2}$ $(yyy\%)$ component, respectively. The high purity of the wave functions establishes for the first time the simulataneous robustness of the Z=50 and N=50 shell closures in ^{100}Sn only $\sim$ 3MeV from the proton dripline corroborating for N=50 the results of Refs.[29, 30] and clearly excludes substantial coupling to the continuum of unbound states.

Acknowledgments

This work was supported by the BMBF under contracts 06MT238 and 06MT9156, by the GSI, by the DFG Cluster of Excellence 153 *Origin and Structure of the Universe*, by the EC within the FP6 through I3-EURONS (contract no. RII3-CT-2004-506065).

[1] K. Langanke, G. Martinez-Pinedo, Rev. Mod. Phys. 75 (2003) 819.

[2] F.T. Avignone, S.R. Elliott, J. Engel, Rev. Mod. Phys. 80 (2008) 481-516

[3] K. Ikeda, S. Fuji and J.I. Fujita, Phys. Lett. B 3 (1963) 271.

[4] I.S. Towner, Phys. Report 155 (1987) 263.

[5] F. Osterfeld, Rev. Mod Phys. 64 (1992) 491.

[6] M. Ichimura, H. Sakai, T. Wakasa, Prog. Part. Nucl. Phys. 56 (2006) 446.

[7] J.C. Hardy, L.C. Carraz, B. Jonson, P.G. Hansen, Phys. Lett. B 71 (1977) 307,

[8] G. Audi, A.H. Wapstra and C. Thibault, Nucl. Phys. A729 (2003) 337.

[9] E. Caurier, G. Martínez-Pindeo, F. Nowacki, A. Poves, A.P. Zuker, Rev. Mod. Phys. 77 (2005) 427.

[10] B.A. Brown, Prog. Part. Nucl. Phys. 47 (2001) 517.

[11] B. Alex Brown, K. Rykaczewski, Phys. Rev. C 50 (1994) R2270.

[12] D.J. Dean, S.E. Koonin, T.T.S. Kuo, K. Langanke, P.B. Radha, Phys. Lett. B 367 (1996) 17.

[13] A. Bobyk, W. Kaminski, and I. N. Borzov, Acta Phys. Pol. B31 (2000) 953.

[14] L. Batist et al., Eur. Phys. J. A 46 (2010) 45.

[15] M. Lewitowicz et al., Phys. Lett 332B (1994) 20.

[16] M. Chartier et al., Phys. Rev. Lett. 77 (1996) 2400.

[17] K. Sümmerer et al., Nucl. Phys. A616 (1997) 341.

[18] A. Stolz et al., Phys. Rev. C 65 (2002) 064603.

[19] D. Bazin et al., Phys. Rev. Lett. 101 (2008) 252501.

[20] H. Geissel et al., Nucl. Instr. Meth. B 70 (1992) 286.

[21] S. Pietri et al., Nucl. Instrum. Meth. B 261 (2007) 1079.

[22] C. Plettner et al., Phys. Rev. C 66 (2002) 044319.

[23] L. Coraggio, A. Covello, A. Gargano, and N. Itaco, Phys. Rev. C 70 (2004) 034310.

[24] M. Hjorth-Jensen, T.T.S. Kuo, E. Osnes, Phys. Rep. 261, 125 (1995) and private communication

[25] D. Seweryniak et al., Phys. Rev. Lett. 99 (2007) 022504.

[26] I.G. Darby et al., Phys. Rev. Lett. 105 (2010) 162502.

[27] I. Hamamoto, H. Sagawa, Phys. Rev. C 48 (1993) R960.

[28] T. Faestermann et al., Eur. Phys. J. A 15 (2002) 185.

[29] A. Blazhev et al., Phys. Rev. C69, 064304 (2004).

[30] P. Boutachkov et al., accepted by Phys. Rev. C

VI. SUPPLEMENTARY INFORMATION

A. Experimental details

1. *Fragment separator (FRS)*

Exotic nuclei were produced via relativistic projectile fragmentation. A ^{124}Xe-beam with an energy of $1AGeV$ per nucleon was directed onto a 4008 mg/cm^2 beryllium target. A production cross section of $5.8(21)pb$ [S1] for ^{100}Sn was determined to be compared with $11(4)pb$ from [S2]. The FRS [S3] was used to separate the various reaction products. It was operated with an achromatic focus at the final focal plane and a wedge shaped aluminium degrader in the dispersive midplane (F2) was inserted to achieve additionally a spatial separation with respect to the mass-to-charge ratio A/Q and the nuclear charge Z of identified ions. In the focal plane F1 after the first quarter of the FRS an additional $2g/cm^2$ Al degrader was placed to keep the countrate at F2 at a tolerable level. Scintillators and tracking ionization chambers at the dispersive midplane (F2) and two multiwire proportional counters and two time-projection chambers at F4 were used to determine the fragments magnetic rigidity $B\rho = (A/Q)m\gamma v$ by measuring its horizontal positions and angles. Multiple time of flight measurements with scintillators at F2 and F4 yielded the velocity v and the Lorentz factor γ and thus the fragments A/Q. The total time of flight was approximately $200ns$ in the fragments rest-frame. At the relativistic energies used here the fragments are completely ionized ($Q = Ze$). An independent determination of the nuclear charge by energy loss measurements in two multiply sampling ionization chambers (MUSIC) at F4 led to an unambiguous identification of the nuclide. Resolutions (FWHM) in mass of $\Delta A = 0.32$ and nuclear charge $\Delta Z = 0.25$ were obtained. At the final focal plane of the FRS the ions were slowed down in a degrader of adjustable thickness and stopped in an implantation detector.

2. *Implantation detector and RISING gamma detection array*

The compact 4π silicon implantation and beta absorber detector (SIMBA) is sensitive to β-, α-, and proton-decay of the heavy ions [S4]. The implantation zone at the center of SIMBA consists of 3 highly segmented $0.7mm$ thick double sided silicon strip detectors with a total number of 1920 pixels per $60mm \times 40mm$ detector. This high granularity enables

correlating the implantation and successive decays of a nucleus for times up to several seconds. In front of and behind the implantation zone stacks of ten $1mm$ thick silicon detectors with lower segmentation were mounted as a total energy calorimeter, stopping beta particles with a maximum energy of $5MeV$ and yielding an average energy resolution of $100keV$ FWHM due to summing up of the energies for an ordinary β decay depositing energy in about 6 silicon layers of SIMBA. The surrounding RISING array for the detection of emitted gamma radiation has an energy resolution of about $3.0keV$ FWHM at $1332keV$ and the absolute photo peak efficiency of the whole setup was about 12% at $662keV$ for gamma radiation originating from the implantation zone.

B. Analysis details

1. Maximum likelihood (MLH) analysis of decay events

Due to an average efficiency of only 60% for correlating implantations with succeeding β-decays and due to the presence of uncorrelated background decays from previous implantations some ambiguity exists in the assignment of each decay event to mother-, daughter-, granddaughter-, and background-decays. All possible scenarios with a maximum number of three decay events during the correlation time have been incorporated in the MLH analysis. The unknown half life of ^{100}Sn was then varied in order to maximize the probability of observing the data sample as it was recorded in the experiment. Considering the probability distribution for each decay event of the entire data sample a total number of 83^{+2}_{-4} of all observed decays can be attributed to decays of ^{100}Sn.

2. Decay gamma ray spectrum and level scheme of ^{100}In

Figure 3 shows the gamma-ray spectrum observed in coincidence with decay events which originate with a probability of 65% from excited states in ^{100}In. A 35% contribution originates from daughter decays or uncorrelated background. The strongest transition from the daughter decay with $1004keV$ is barely visible in the spectrum. Furthermore none of the visible gamma-rays corresponds to lines in a high statistics spectrum obtained from uncorrelated background decays. The observed intensities are within the very limited statistics all consistent with ~ 70 ^{100}Sn decays corresponding to a correlation window of 4 seconds.

The proposed scenario of the depopulation of excited states in ^{100}In as shown in Figure 4 is consistent with the observation of a total gamma-ray energy of 2.76(43) MeV measured with a total absorption BGO-detector [S2] in a former experiment. In addition, the measured mass difference of ^{100}Sn and ^{100}In [S5] combined with our measured Q_{EC} value of 3.29 MeV yields an excitation energy of the 1^+ state of 2.6(10) MeV. A third indication is the observation of one ^{100}Sn decay event, where 1.49 MeV has been deposited in a single pixel in coincidence with a β particle track. Since a β-particle cannot deposit that much energy we attribute this event to a β-delayed proton emission. Subtraction of the average energy deposited by a β-particle in a single pixel of 0.17(14) MeV yields a proton energy of 1.32(14) MeV. The natural assumption is that the 1^+ state, fed by β-decay, is depopulated to a fraction $< 1\%$ by a proton decay to the ^{99}Cd ground state. By adding the proton separation energy of ^{100}In $S_p = 1.61(31)MeV$ [S6] we arrive at an excitation energy of the 1^+ state in ^{100}In of 2.93(34) MeV. For the partial proton-decay half-life we estimate [S7] 40ps with more than a factor of 10 uncertainty for an L=2 transition to the $5/2^+$ ground state of ^{99}Cd. This is about a factor 10^4 larger than for a 2048 keV $M1$-transition with 1 Weisskopf unit. Thus a proton decay branch in the range of 0.1% to 1.0% is not unexpected.

3. Determination of the beta endpoint energy

For all decay events which could be assigned to a ^{100}Sn decay with a probability of at least 75% the uninterrupted traces of the decay positrons in the implantation detector were reconstructed and checked for integrity, i.e. for possible positron escapes with incomplete energy deposition and interference of the trace with single Compton events of gamma rays emitted in coincidence. The beta spectrum resulting from the summed up energies shown in Figure 5 was fitted using a MLH analysis based on a single component beta decay phase space function to determine the beta endpoint energy in the decay of ^{100}Sn. The region below $400keV$ was neglected to avoid the narrow structure (7 counts) around $250keV$, whose origin is only partially understood. Two decays within this region which occured without a coincident observation of any gamma radiation might be attributed to uncorrelated background noise rather than real decay events since these low energies are not far from the trigger threshold. Another two events might come from electron capture decays of ^{100}Sn (fraction 13%) accompanied by an energy deposition in the spatial three dimensional correlation win-

dow originating from Compton scattered gamma rays emitted during the depopulation of excited states in the daughter nucleus ^{100}In. Thus the narrow structure around $250keV$ has a large systematic uncertainty and was not considered in the fitting procedure. The MLH fit of the end-point energy would be strongly influenced by the highest energy events, since obviously the end-point of a one component phase space would have to be higher than the highest energy events. However, one cannot exclude that the few events with energies above $2600keV$ could originate from the daughter (probability 13%) and uncorrelated background decays (probability 12%). Therefore these high energy events were also excluded from the MLH fit. However, the choice of the upper limit for the fit in the tail of the distribution as indicated in Figure 5 has only a weak influence on the result which is much less than the statistical uncertainty.

The corresponding fraction of electron capture decays was calculated from the determined beta endpoint energy to be 13% of all ^{100}Sn decays [S8].

C. Interpretation of the data

1. Compilation of various predictions for the GT-strength in the decay of ^{100}Sn

The basic estimate for the GT-strength in the decay of ^{100}Sn comes from the extreme single particle shell model (ESPM) where no correlations between the nucleons are taken into account. The GT transition strength is given by $B_{GT}^{ESM} = \frac{4\ell}{2\ell+1} \cdot (1 - \frac{N_{\nu g7/2}}{8}) \cdot N_{\pi g9/2}$ [S9]. $\ell = 4$ denotes the involved orbital angular momentum. $N_{\pi g9/2} = 10$ and $N_{\nu g7/2} = 0$ are the occupation numbers of the initial proton orbital and the final neutron orbital, respectively. The extreme single particle estimate increases linearly with the orbital angular momentum ℓ, and takes its maximum value for a given ℓ for a filled $\ell + 1/2$ and empty $\ell - 1/2$ orbit. The constraints for observing the maximum value in β^+/EC decay are given by the line of stability and the proton dripline which exlude doubly magic nuclei below and above N=Z=50 from observation making ^{100}Sn a unique case in the Segré chart.

The experimental B_{GT} value is substantially lower than the pure single particle estimate of $B_{GT,sp} = 17.78$, which assumes the decay of one of the $N_\pi = 10$ protons occupying the full $g_{9/2}$ orbital into an empty $g_{7/2}$ neutron orbital with $N_\nu = 0$. This is not unexpected since particle-hole correlations within the full *gds* shell as well as short range correlations shifting

strength to even higher energies would lead to a reduced GT-strength.

Table I summarizes various theoretical results for the prediction of the GT strength in the decay of ^{100}Sn. The quenched values are obtained by multiplying the square of the quenching factor to the Gamow-Teller strength.

Model	Ref	unquenched	quenched	quenching factor
ESPM	[S9]	17.78	10.00	0.75
MCSM	[S10]	10.3	6.5	0.79
QRPA	[S11]	8.95		
FFS	[S11]	7.63		
extrapol.	[S12]	9.8	5.2	0.75
SM+corr.	[S13]	14.2		
LSSM	this work	~ 13.90	~ 7.82	0.75
LSSM (only 1_1^+)	this work	10.10	5.68	0.75

TABLE I: Predicted B_{GT} values of the strength accessible in the Q_{EC} energy window in the decay of ^{100}Sn. The measured B_{GT} is $9.1^{+4.8}_{-2.3}$ assuming a single final state dominantly populated in the decay of ^{100}Sn.

2. Details of shell model calculations

The large scale shell model (LSSM) calculations in this work for the determination of the ^{100}In level scheme and for the determination of the GT-strength distribution in the decay of ^{100}Sn depending on possible final states in the daughter nucleus ^{100}In were performed in the proton-neutron $\pi\nu(g, d, s)$ model space with a ^{80}Zr core making use of the Strasbourg codes ANTOINE and NATHAN [S14, S15]. Up to 5 particle - 5 hole excitations ($5p5h$), truncation level $t = 5$, across the Z,N=50 closed shells were allowed. The interaction was derived from the CD-Bonn nucleon-nucleon (NN) potential [S16], starting from a G-matrix including folded diagrams and higher order in-medium corrections for this model space according to the prescription of Ref. [S17]. Starting from a global prediction for single particle energies

for a hypothetical (spherical) ^{80}Zr core [S18] monopole corrections were applied to reproduce extrapolated single particle/hole energies for ^{100}Sn [S19] including a shell gap of 6.50 MeV for both protons and neutrons. For details see Ref. [S20] where this approach was verified for core excited states in ^{98}Cd. Recently additional support was obtained from the description of a core excited isomer in ^{96}Ag [S21].

The resulting ^{100}In level scheme relevant for the decay pattern of the 1^+ state is shown in Figure 4 of the main text. E2 polarisation charges δe= 0.5e and effective spin g-factors $g_s^{eff} = 0.75 g_s^{free}$ and orbital corrections $\delta g_l = \pm 0.1$ for protons and neutrons were used for M1 transitions. The γ decay pattern of the first 1^+ state in this model space as calculated from transition strengths excludes E2 transitions in competition to M1 and may be used as guideline to arrange the experimentally observed γ rays in a tentative level scheme. The disparate branching from the first 1^+ state of dominant configuration $\pi g_{9/2}^{-1}\, \nu g_{7/2}$ to the $2^+_{1,2}$ states in the LSSM calculations may be due to the neglect of l-forbidden M1 transitions as the daughter states have different partitions of the $\pi g_{9/2}^{-1}\, \nu g_{7/2}$ and $\pi g_{9/2}^{-1}\, \nu d_{5/2}$ configurations.

The quenched GT distribution, as shown in Figure 1 of the supplementary section, is used to correct the total GT strength for the part observable in the Q_{EC} window. Note the multiple 1^+ states above the dominantly populated 1^+_1. The states 1^+_{2-4} between 3.5 and 4.0 MeV carry 21% of the total strength while the 1^+_1 receives 69% of the total strength. Nevertheless due to the reduced phase space factor the former is not accessible to the present experiment.

The total quenched GT strength in an energy window of up to 60MeV for excited states in the daughter nucleus yields a value of 8.19. With a quenched GT-strength of 7.82, in the Q_{EC} window of 7.03(20) MeV most of the strength is concentrated. The value determined for the first excited 1^+ state is 5.68.

3. Interpretation of the measured GT-strength B_{GT}

According to the large scale shell model (LSSM) calculations it is reasonable to consider that a few 1^+ states in ^{100}In are populated in the decay of ^{100}Sn with the corresponding distribution of the Gamow-Teller strength B_{GT} as shown in Figure 1 of the supplementary section. If we assume from the LSSM calculation the four lowest 1^+ states in ^{100}In with the same energy splitting and the same relative GT-strength, the measured beta-spectrum

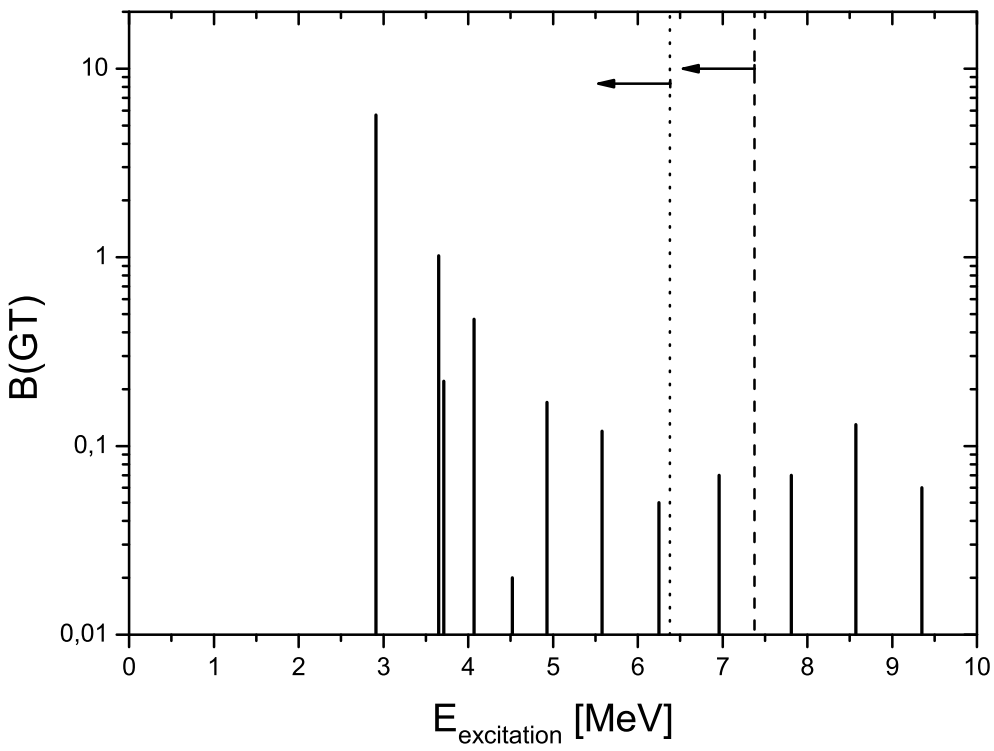

FIG. 1: LSSM calculation of the distribution of the quenched GT-strength in the decay of ^{100}Sn depending on the exciation energy of possible final 1^+ states in the daughter nucleus ^{100}In. The standard renormalisation factor of 0.75 of the GT-operator was applied to account for short-range correlations. The dashed line indicates the energy window accessible in EC-decays and the dotted line shows the energy window accessible in β^+ decays, respectively.

would yield an endpoint energy for the transition to the lowest 1^+ state that is larger by $73keV$. This is due to the shift of the centroid of the β-spectrum to lower energies induced by the minor contribution of the feeding of the higher lying 1^+ states in contrast to the assumption that only a single final state is populated.

The corrected value of the beta-endpoint energy together with the corrected partial half life would result in a $B_{GT}(1_1^+) = 7.6^{+2.6}_{-2.1}$, a factor of 1.3 larger than the result of the LSSM calculation of 5.68, which is still within the uncertainties. The summed GT-strength is $\sum_{i=1}^{4} B_{GT}(1_i^+) = 9.9^{+3.4}_{-2.8}$ in comparison to the LSSM value of 7.40.

[S1] K. Straub, Dissertation TU München, (2011), K. Straub et al., to be published

[S2] K. Sümmerer et al., Nucl. Phys. A616 (1997) 341.

[S3] H. Geissel et al., Nucl. Instr. Meth. B 70 (1992) 286.

[S4] Ch. Hinke, Dissertation TU München, (2010).

[S5] M. Chartier et al., Phys. Rev. Lett. 77 (1996) 2400.

[S6] G. Audi, A.H. Wapstra and C. Thibault, Nucl. Phys. A729 (2003) 337.

[S7] D.S.Delion, R.J. Liotta, and R. Wyss, Phys. Rev. Lett. 96 (2006) 072501.

[S8] Web-interface LOGFT at http://www.nndc.bnl.gov/logft/ based on N.B. Gove and M.J. Martin., Nuclear Data Tables A10 (1971) 206

[S9] A. de Shalit, I. Talmi, Nuclear Shell Theory, Academic Press, New York and London, 1963

[S10] D.J. Dean, S.E. Koonin, T.T.S. Kuo, K. Langanke, P.B. Radha, Phys. Lett. B 367 (1996) 17.

[S11] A. Bobyk, W. Kaminski, and I. N. Borzov, Acta Phys. Pol. B31 (2000) 953.

[S12] L. Batist et al., Eur. Phys. J. A 46 (2010) 45.

[S13] B. Alex Brown, K. Rykaczewski, Phys. Rev. C 50 (1994) R2270.

[S14] E. Caurier and F. Nowacki, Act. Phys. Pol. B 30, 705 (1999).

[S15] E. Caurier, G. Martínez-Pinedo, F. Nowacki, A. Poves, A. P. Zuker, Rev. Mod. Phys. 77, 427 (2005).

[S16] R. Machleidt, Phys. Rev. C 63, 024001 (2001).

[S17] M. Hjorth-Jensen, T.T.S. Kuo, E. Osnes, Phys. Rep. 261, 125 (1995) and private communication.

[S18] J. Duflo and A.P. Zuker, Phys. Rev. C59, R2347 (1999).

[S19] H. Grawe and M. Lewitowicz, Nucl. Phys. A693, 116 (2001).

[S20] A. Blazhev et al., Phys. Rev. C69, 064304 (2004).

[S21] P. Boutachkov et al., accepted by Phys. Rev. C